PROCEEDINGS, 44th Workshop on Geothermal Reservoir Engineering
Stanford University, Stanford, California, February 11-13, 2019
SGP-TR-214

Numerical Modeling and Laboratory Experiments on a Propagating Hydraulic Fracture Intersecting with a Preexisting Fracture

Ayaka Abe[1], Takuya Ishibashi[2], Hiroshi Asanuma[2], and Roland N. Horne[1]

[1]Department of Energy Resources Engineering, Stanford University, Stanford, California, 94025, USA

[2]Fukushima Renewable Energy Institute, AIST, Koriyama, Fukushima, 963-0298, Japan

aabe@stanford.edu

Keywords: enhanced geothermal systems, hydraulic stimulation, numerical modeling and simulation, laboratory experiments

ABSTRACT

Modeling realistic fracture networks is necessary for characterizing a geothermal reservoir because the permeability of reservoir formations is low and fractures are the main pathways of geothermal fluid. Hydraulic stimulation in a geothermal reservoir occurs both by creating new hydraulic fractures and by stimulating preexisting natural fractures. Analyzing the interaction between preexisting fractures and newly created fractures during hydraulic stimulation is thus necessary to better understand the creation of a fracture network. Microseismic data during hydraulic stimulation show broad clouds that indicate the creation of complex fracture networks, suggesting that hydraulic fractures may branch, terminate, and continue propagating when they intersect with natural fractures. To understand this kind of hydraulically induced fracture network, knowing how a propagating hydraulic fracture interacts with a preexisting natural fracture is necessary.

In this work, a numerical model using fracture mechanics was developed and used to investigate how hydraulic fractures and preexisting natural fractures interact. We extended the analytical work on the cross/terminate criteria for orthogonally intersecting fractures developed by Renshaw and Pollard (1995) and the results show a good agreement with experimental data in past work. In addition, to study this problem in a laboratory scale experiment, we used a 3D printer to create artificial core samples containing a preexisting interface and an initial hydraulic fracture, and then applied axial stress and confining pressure using a triaxial loading system. The experimental results were compared both to the numerical results developed in this work and to the analytical work on the cross/terminate criteria for orthogonally intersecting fractures by Renshaw and Pollard (1995). In our experiments, a hydraulic fracture was initiated and propagated to an existing orthogonal precut fracture. The propagating hydraulic fracture crossed the precut with higher axial stress but terminated with lower axial stress, in agreement with the numerical work. With this work, we also suggest the possibilities of using 3D-printed core samples for more complex fracturing experiments. This work demonstrates the utility of 3D-printed core samples for studying fracture network creation, and raises the possibility of modeling more complex fracture networks in future laboratory experiments.

1. INTRODUCTION

Hydraulic stimulation is performed in EGS reservoirs to enhance reservoir permeability. The main mechanisms of reservoir permeability enhancement are shear dilation of preexisting natural fractures, creating new fractures, and fracture connectivity enhancement. A microearthquake cloud expands during a hydraulic fracture treatment as fluid pressure in the reservoir increases, causing preexisting natural fractures to slide in shear. In the EGS experiment at Fenton Hill, New Mexico, a single hydraulic fracture was expected to be created by the hydraulic stimulation treatment (Brown et al., 2012). However, the microearthquake cloud observed during stimulation treatment grew broadly in a NNW-SSE direction (Norbeck, 2016). If hydraulic fractures dominate, the microearthquake cloud would be expected to propagate perpendicular to the least principle stress (N30°E), but this did not happen in the field. Moreover, the injection pressures during the stimulations exceeded the least principal stress significantly (Norbeck et al., 2016). This implies that hydraulic fractures were created in the reservoir, suggesting that reservoir stimulation occurred both by creating new hydraulic fractures and by shear dilation of existing fractures. This mixed-mechanism stimulation has been suggested by Weng et al. (2011) in the application of hydraulic fracturing in shale gas reservoirs. This has also been proposed to be the dominant mechanism of stimulation in geothermal reservoirs in many EGS projects (McClure & Horne, 2014).

In a mixed-mechanism stimulation, newly created mode-I fractures intersect with preexisting natural fractures, which creates various patterns of connections. In addition to this, McClure and Horne (2014) suggested that hydraulic fractures may splay out from a natural fracture. Injection pressure in an EGS shear stimulation is usually higher than the least principal stress, meaning that the pressure is high enough to initiate new hydraulic fractures. It is difficult to initiate new fractures as granite has high tensile strength, but preexisting natural fractures slide and dilate at lower pressure than required for initiation of a new fracture. Therefore it is highly probable that new fractures are created from the tips of stimulated preexisting natural fractures as stress concentrates at the crack tips (McClure, 2014).

Although these mixed-mechanism fracture propagation patterns have been suggested based on field observation, how fractures actually propagate and create a fracture network is less clear and still being actively investigated. Thus far, analytical and experimental research that discusses fracture intersection criteria that focus on fracture propagation in mode-I, mode-II, and the mixed mechanism of mode-I and mode-II has been mainly done in oil and gas settings. For example, Olson (2008) showed a complex fracture network model including the hydraulic fracture with the effect of stress shadow and natural fractures in unconventional oil and gas settings. Physics-based

approaches including fluid flow and geomechanics that can simulate fracture propagation and stimulation in field scale will give insight into many outstanding questions about fracture network creation.

In this work, as an approach to model hydraulic stimulation in an EGS reservoir, how fractures propagate and intersect with each other was investigated both numerically and experimentally.

2. PROPAGATING FRACTURE INTERSECTING TO ANOTHER FRACTURE

How hydraulic fractures intersect with preexisting natural fractures has been studied analytically, numerically, and experimentally especially in unconventional oil and gas settings. In these kinds of reservoirs, hydraulic fractures dominate the fracture network, and thus microseismic events occur and a cloud expands along the direction perpendicular to the least principle stress. In an EGS reservoir, in contrast, the microseismic cloud expands broadly, indicating that natural fracture orientations and distribution are also key factors that affect hydraulic fracture treatment design (Norbeck, 2016). Indeed, unlike in unconventional oil and gas reservoirs, in EGS reservoirs, larger natural fractures dominate the fracture networks because the matrix rock is stiffer and natural fractures are larger compared to those in unconventional oil and gas reservoirs.

In this paper, a numerical method to determine whether a propagating mode-I fracture crosses or follows a preexisting natural fracture with an arbitrary intersection angle is suggested based on the propagation criterion for an orthogonal intersection developed by Renshaw and Pollard (1995), and the results are compared to lab experimental results from the literature.

2.1 Analytical Models

Analytical models for the propagation criterion were developed by Renshaw and Pollard (1995) for an orthogonal intersection and later extended for a nonorthogonal intersection (Gu & Weng, 2010; Gu et al., 2011). Renshaw and Pollard (1995) conducted theoretical and experimental work to analyze the mechanism of younger fractures propagating across older fractures oriented perpendicular to the approaching fracture. They stated the criterion as "compressional crossing will occur if the magnitude of the compression acting perpendicular to the frictional interface is sufficient to prevent slip along the interface at the moment when the stress ahead of the fracture tip is sufficient to initiate a fracture on the opposite side of the interface". The stress field induced by the fracture tip was calculated and the condition where the slip along the frictional interface would not occur based on the Mohr–Coulomb failure criterion was derived. Their model is based on the linear elastic fracture mechanics solution for the stresses near a fracture tip and calculates the stresses needed to cause slip on the preexisting interface. Gu and Weng (2010) applied the criterion for a fracture approaching a frictional interface at a nonorthogonal angle. The authors later verified their model with laboratory tests (Gu et al., 2011).

The singular stress field ahead of a crack tip under mode-I loading in an isotropic linear elastic material under the plane-strain condition are expressed in closed form (Anderson, 2005):

$$\sigma_{xx}^{(I)} = \frac{K_I}{\sqrt{2\pi r}}\cos\frac{\theta}{2}\left(1 - \sin\frac{\theta}{2}\sin\frac{3\theta}{2}\right) \quad (1)$$

$$\sigma_{yy}^{(I)} = \frac{K_I}{\sqrt{2\pi r}}\cos\frac{\theta}{2}\left(1 + \sin\frac{\theta}{2}\sin\frac{3\theta}{2}\right) \quad (2)$$

$$\sigma_{xy}^{(I)} = \frac{K_I}{\sqrt{2\pi r}}\cos\frac{\theta}{2}\sin\frac{\theta}{2}\cos\frac{3\theta}{2} \quad (3)$$

where K_I is the mode-I stress intensity factor, r and θ are the polar coordinate with the origin at the fracture tip. Based on the principle of superposition, the total stress field caused by the remote stresses and the singular stress field are:

$$\sigma_{ij}^{(total)} = \sigma_{ij}^{(remote)} + \sigma_{ij}^{(I)} \quad (4)$$

Maximum magnitude of the stress components is found at the critical radius $r = r_c$ where the least principal stress is the same as the tensile strength. The area within $r = r_c$ is referred to as the *fracture process zone* where the inelastic deformation exists. Then the normal stress and the shear stress along the frictional interface were calculated and plugged in to the Mohr–Coulomb failure criterion:

$$|\sigma_s| < \mu\sigma_n + S_0 \quad (5)$$

Then they derived the crossing/terminating threshold for the fracture intersecting the fracture with $\theta = \frac{\pi}{2}$ as:

$$\frac{-\sigma_{xx}^r}{T_0 - \sigma_{yy}^r} > \frac{0.35 + \frac{0.35}{\mu}}{1.06} \quad (6)$$

where σ_{xx}^r *and* σ_{yy}^r are remote stresses, and μ is the frictional coefficient of the fracture.

In the fracture crossing criterion by Gu and Weng (2010), a hydraulic fracture crosses a preexisting interface when shear stress acting on the preexisting fracture at the point where $\sigma_{yy} = T_0$ with $\geq \frac{\pi}{2}$ is smaller than the Mohr–Coulomb failure criterion.

$$\sigma_s = \mathrm{K}\sin\frac{\theta}{2}\sin\frac{3\theta}{2}\sin 2\theta + K\sin\frac{\theta}{2}\cos\frac{3\theta}{2}\cos 2\theta - \frac{S_{Hmax} - S_{hmin}}{2}\sin 2\theta \quad (7)$$

$$\sigma_n = \mathrm{K} + \mathrm{K}\sin\frac{\theta}{2}\sin\frac{3\theta}{2}\cos 2\theta - K\sin\frac{\theta}{2}\cos\frac{3\theta}{2}\sin 2\theta + \frac{S_{Hmax} + S_{hmin}}{2} - \frac{S_{Hmax} - S_{hmin}}{2}\cos 2\theta \quad (8)$$

where σ_n and σ_s are the normal and shear stresses acting on the preexisting natural fracture near the crack tip respectively, μ is the frictional coefficient, S_0 is the cohesion of the interface, K represents the stress level required to reinitiate a fracture on the other side of the interface, θ is the angle between the propagating fracture and preexisting fracture, S_{Hmax} is the maximum principal stress, and S_{hmin} is the minimum principal stress. When the interface slips, the propagating fracture cannot initiate fracturing on the other side of the interface surface, and the propagation stops.

2.2 Methodology

Numerical work to investigate whether a propagating fracture crosses another fracture with an arbitrary angle was done by applying the criterion for fracture crossing stated by Renshaw and Pollard (1995) that crossing will occur if the slip along the frictional interface would not occur. When the stress caused by a propagating fracture tip is sufficient to initiate a fracture on the interface, a part of the interface needs to be inside the fracture process zone, which follows the assumption of Wu and Pollard (1992) that the stress concentrating flaw such as an asperity or a notch along a fracture surface reinitiates a fracture. The segment along the interface within the fracture process zone where there is a possibility to initiate a fracture will be termed a "*fracture-chance segment*" (Figure 1).

The fracture process zone is determined as the area inside the line of $\sigma_1 = -T_0$ (Figure 1). The stresses inside the fracture process zone are assumed to be equal to or less than the yield stress (Segall, 2010). In this work, the stress inside the fracture process zone is assumed to be equal to the tensile strength. Therefore the linear elastic fracture mechanics is applied inside the fracture process zone. A mode-I fracture tip induces the tension field expressed in Equations (1), (2), (3), and (4). Then the principal stresses are expressed by the following:

$$\sigma_1 = \frac{\sigma_{xx}+\sigma_{yy}}{2} + \sqrt{\left(\frac{\sigma_{xx}-\sigma_{yy}}{2}\right)^2 + \sigma_{xy}^2} \tag{9}$$

$$\sigma_2 = \frac{\sigma_{xx}+\sigma_{yy}}{2} - \sqrt{\left(\frac{\sigma_{xx}-\sigma_{yy}}{2}\right)^2 + \sigma_{xy}^2} \tag{10}$$

$$\theta_p = \frac{1}{2}\tan^{-1}\frac{2\sigma_{xy}}{\sigma_{yy}-\sigma_{xx}} \tag{11}$$

where σ_1 and σ_2 are the maximum and least principal stresses respectively, σ_{ij} is the total stresses, and θ_p is the direction of the maximum principal stress (Pollard & Fletcher, 2005).

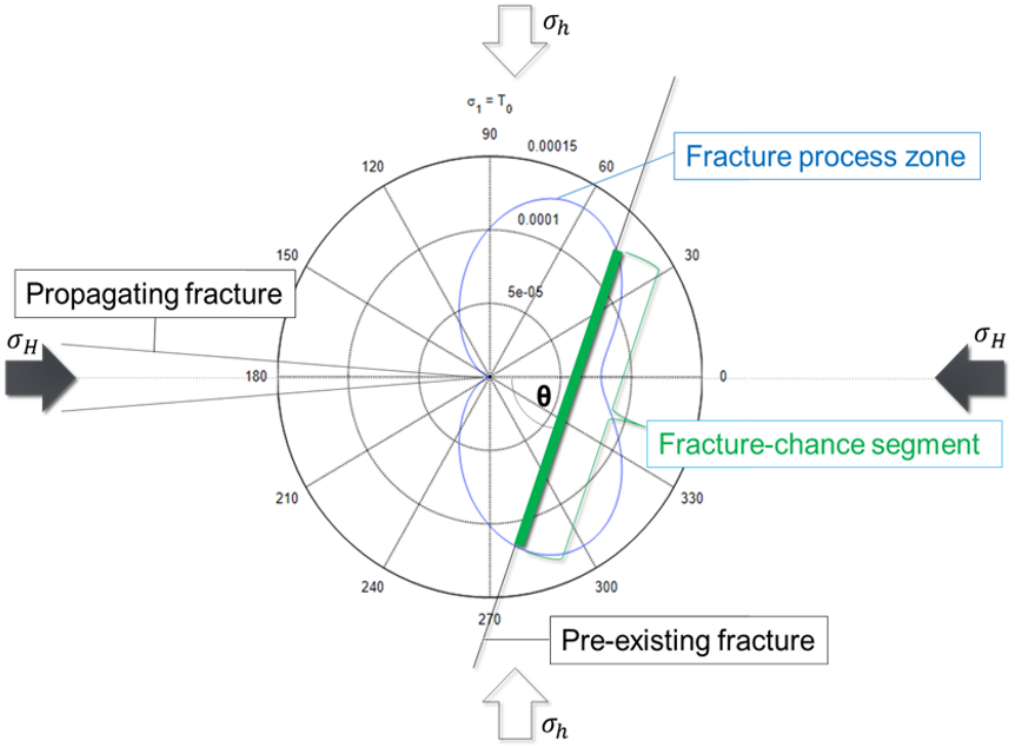

Figure 1: An example of a fracture process zone and fracture-chance segment (σ_{xx}= 70MPa, σ_{yy}= 35MPa, σ_{xy}= 0MPa, and T_0= -10MPa). Fracture-chance segment is shown in green line, fracture process zone is the area surrounded by the blue line. A mode I fracture is located at x < 0 and y = 0.

In this numerical work, the fracture-chance segment was divided into a sufficient number of small segments. To check if $|\sigma_s| < \mu\sigma_n + S_0$ and $\sigma_n > 0$ are satisfied at all the segments along the fracture-chance segment, the normal stress and shear stress acting on each segment are calculated by:

$$\sigma_n = \sigma_{xx} \sin^2\theta - 2\sigma_{xy} \sin\theta \cos\theta + \sigma_{yy} \cos^2\theta \tag{12}$$

$$\sigma_s = -(\sigma_{xx} - \sigma_{yy}) \sin\theta \cos\theta + \sigma_{xy}(\cos^2\theta - \sin^2\theta) \tag{13}$$

where σ_{ij} are the total stresses and θ is the fracture angle to σ_H.

There are three patterns that would occur when a hydraulic fracture approaches a preexisting fracture:

Pattern 1) $|\sigma_s| < \mu\sigma_n + S_0$ and $\sigma_n > 0$ are satisfied along the entire fracture-chance segment. This means that the induced stress field ahead of a crack tip causes neither slip nor opening along a preexisting fracture. Consequently, the propagating hydraulic fracture is expected to cross the preexisting fracture,

Pattern 2) $|\sigma_s| < \mu\sigma_n + S_0$ and $\sigma_n > 0$ are not satisfied along the entire fracture-chance segment. This means that the induced stress field occurring ahead of a crack tip causes slip or opening along the preexisting fracture inside the fracture process zone. The propagating hydraulic fracture is hence expected to follow the preexisting fracture.

Pattern 3) $|\sigma_s| < \mu\sigma_n + S_0$ and $\sigma_n > 0$ are not satisfied on a part of the fracture-chance segment. This means that the induced stress field ahead of a crack tip partially causes slip or opening along the preexisting fracture inside the fracture process zone.

2.3 Comparison with Lab Experiment Data

To verify this numerical method, data from laboratory experiments in previous studies were compared. Those lab experiments showed whether a propagating mode-I fracture, either initiated by hydraulic fracturing or a point force, crossed or terminated at a frictional interface with varied intersection angles and stress state. The numerical results were compared to the lab experiment results of Blanton (1982), Warpinski and Teufel, (1987), Zhou et al., (2008) and Gu and Weng (2010).

As Table 1 shows, with the pattern 1 where any region of the fracture-chance segment neither opens nor slides, a propagating fracture crosses a frictional interface in all the cases in the lab experiment results. Moreover, with the pattern 2 where any region of the fracture-chance segment opens or slides, a propagating fracture follows a frictional interface in all cases. On the other hand, when the results from the numerical method show that the induced stress field partially causes slip or opening along the fracture-chance segment, then in roughly half of the cases, a propagating fracture crosses the frictional interface.

Table 1: Comparison with Lab Experiment Results

Numerical Results	Lab Experiment Results	
	crosses	follows
1) Entire fracture-chance segment does not open nor slide $\|\sigma_s\| < \mu\sigma_n + S_0$ and $\sigma_n > 0$	11	0
2) Entire fracture-chance segment opens or slides $\|\sigma_s\| > \mu\sigma_n + S_0$ or $\sigma_n < 0$	0	20
3) A part of the fracture-chance segment opens or slides Partially $\|\sigma_s\| > \mu\sigma_n + S_0$ or $\sigma_n < 0$	3	5

2.4 The Offset of Discontinuous Crossing

Helgeson & Aydin, (1991) reported a field observation of joint propagation in layered sedimentary rocks that shows offset at a discontinuous crossing of fractures. This is not an uncommon observation in the field. Such observations support the concept of reinitiation with spatial offsets between fracture segments on either side of the interface, occuring when a fracture crosses a frictional interface (Renshaw & Pollard, 1995). Following the assumption by Renshaw and Pollard (1995) that discontinuous crossing requires less compression than continuous crossing, and reinitiation occurs at an asperity or a notch on the surface of a frictional interface where the maximum principal stress is equal to the tensile strength, the offset of a discontinuous crossing can be calculated analytically.

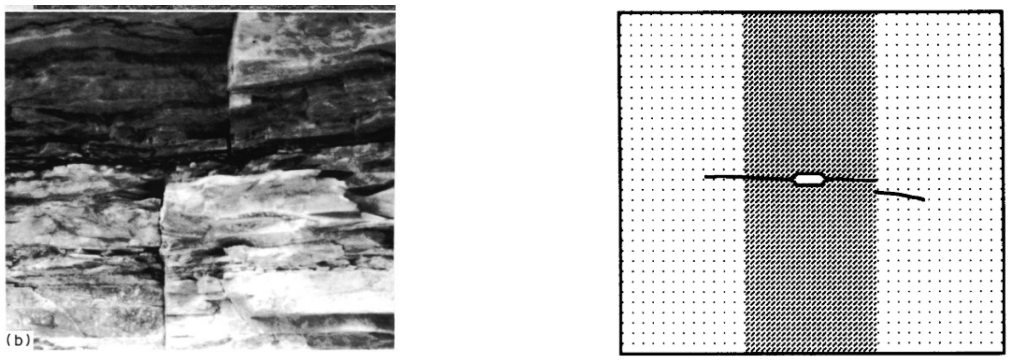

Figure 2: (Left) An example of disconsinuous crossing observed in the field, (Right) A skech of a sample showing both continuous and disconsinuous crossing (Renshaw & Pollard ,1995)

The singular stress field ahead of a crack tip under mode-I loading in an isotropic linear elastic material under the plane-strain condition can be expressed in the closed form (Anderson, 2005):

$$\sigma_{yy}^{(I)} = \frac{K_I}{\sqrt{2\pi r}} \cos\frac{\theta}{2}\left(1 + \sin\frac{\theta}{2}\sin\frac{3\theta}{2}\right) \tag{14}$$

At r $= r_c$, the stress acting parallel to the fracture surface is equal to T_0, and then, assuming $\theta = \frac{\pi}{2}$ and $K_I = K_{Ic}$ as a hydraulic fracture is propagating, the offset r_c is expressed as:

$$\sigma_{yy}^{c} = T_0 - \sigma_{yy}^{r} = \frac{K_{Ic}}{\sqrt{2\pi r_c}} \cos\frac{\pi}{4}\left(1 + \sin\frac{\pi}{4}\sin\frac{3\pi}{4}\right) \tag{15}$$

$$r_c = \frac{9}{16\pi}\frac{K_{Ic}}{T_0 - \sigma_{yy}^{r}} \tag{16}$$

where σ_{yy}^{r} is the least principal stress. Figure 3 shows that the distance of the offset assuming that the preexisting fracture surface at 90 degrees. In a high compressive stress state such that $T_0 - \sigma_{yy}^{r}$ is larger than 40MPa, the offset would be less than 0.1mm, which is almost not visible. It would be possible to estimate the magnitude of remote stress σ_h.from the offset length when the offset is visible.

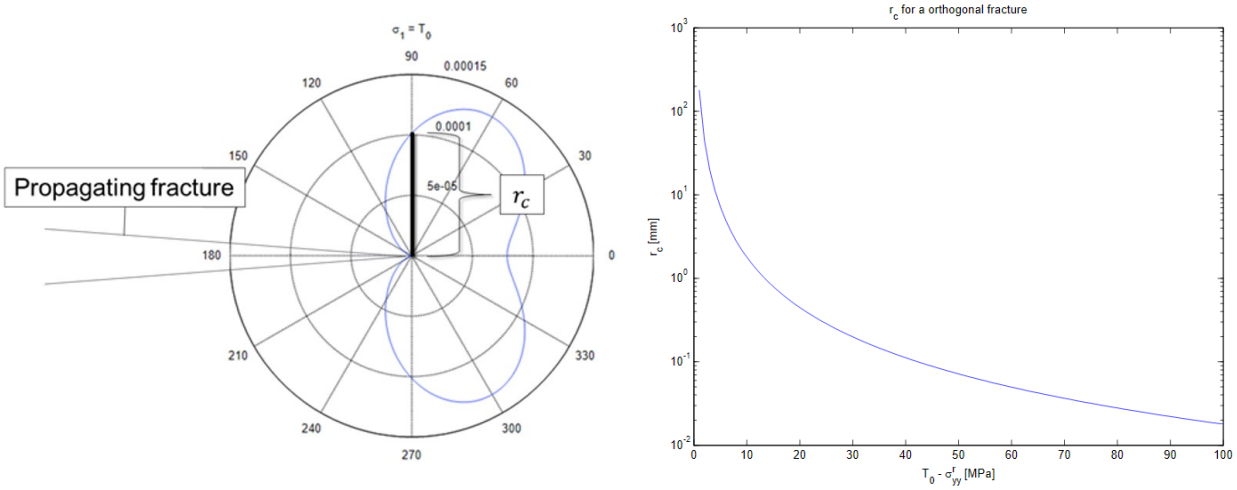

Figure 3: (Left) Discontinuous offset length r_c, (Right) The relationship between discontinuous offset length and $T_0 - \sigma_{yy}^{r}$ ($K_{Ic} = 1\text{MPa} \cdot \sqrt{m}$).

2.3 Discussion

The results of this comparison indicate that the numerical method shows a significantly good agreement with the experimental results in past work, especially when the numerical result shows that the entire fracture-chance segment satisfies $|\sigma_s| < \mu\sigma_n + S_0$ and $\sigma_n > 0$ and when the entire fracture-chance segment does not satisfy these criteria. When a part of the fracture-chance segment does not satisfy $|\sigma_s| < \mu\sigma_n + S_0$ or $\sigma_n > 0$, then it could be said that in half of the cases a propagating fracture would cross the frictional interface.

In the experimental results in past work, rocks that typically have homogeneous isotropic properties such as sandstone, cement, and hydrostone were used, and the preexisting frictional interfaces were ground smooth. In actual field conditions, local heterogeneity, such

as the tensile strength varying at a small scale, grain size distribution, or the stress concentrating flaws such as an asperity or a notch along a fracture would affect the result. Chen et al., (2018) investigated a hydraulic fracture propagation intersecting a cemented preexisting natural fracture by DEM. They suggested that the material properties of the cement and matrix rock affect whether a hydraulic fracture keeps a straight trajectory or branches into the cemented natural fracture. These effects by cemented natural fractures should be considered when modeling fracture network creation.

3. LABORATORY SCALE EXPERIMENTS USING 3D PRINTED CORE SAMPLES

The purpose of these experiments was to verify the method to determine how a propagating fracture intersects a preexisting fracture at varied angles. Another purpose was to explore the possibility of using a 3D-printed core sample for hydraulic fracturing experiments. The advantages of using a 3D-printed core sample are: 1) the semitransparent material enables monitoring of fracture propagation and intersection; 2) using the 3D printer makes it easy to design a core sample with well-controlled fracture geometry; and 3) the material is homogeneous and impermeable.

The experimental design is explained in the following sections in detail. Briefly, in these experiments, a hydraulic fracture was initiated by injecting water and the initiated hydraulic fracture intersected a preexisting cut inside the 3D-printed core sample. Fracture intersection angle was 90 degrees. The confining pressure was kept constant and the axial stress was changed to observe the relationship between the stress state and the fracture cross/follow condition. Water pressure was applied until a hydraulic fracture was initiated and the pressure was reduced immediately after the fracture was initiated.

3.1 Sample Materials

The samples used in this study were made using a 3D printer, KEYENCE Agilista-3100. The sample size is 50.0mm diameter by 50.0mm height made of transparent plastic AR-M2. Mechanical properties of the material are listed in Table 2. The matrix is impermeable and totally homogeneous.

A cut was printed at the height of 40.0mm from the bottom. This cut acts as a preexisting natural fracture that is crossed by a propagating hydraulic fracture. The surfaces of the cut were ground for 2 minutes on an Ibaraki granite block. Naniwa Abrasive Coarse Grain GC #30 was used. An initial crack was printed on the bottom. The geometry of the initial crack is a half ellipsoid whose principal semiaxes are 20.0mm, 30.0mm, and 0.5mm.

Table 2: Sample material properties

Property	Value	Unit
Tensile strength	40-55	MPa
Compressive strength	70-80	MPa
Bending strength	60-80	MPa
Young's modulus	1.8-2.1	GPa
Flexural modulus	1.9-2.4	GPa

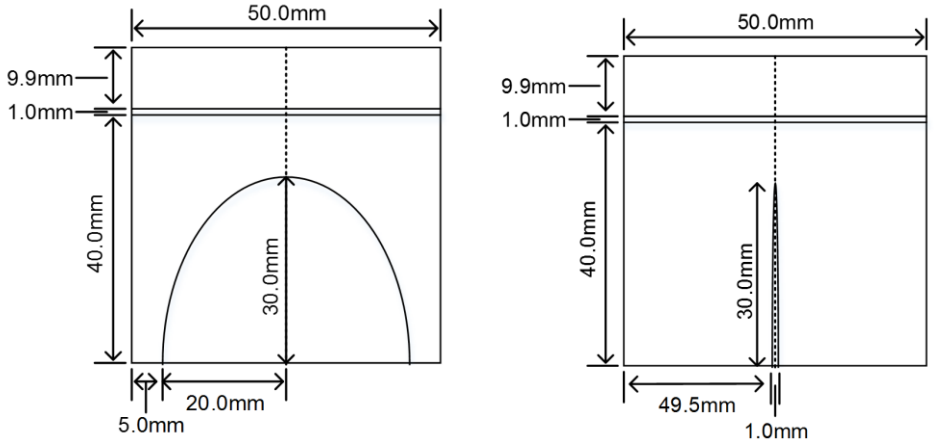

Figure 4: Sketches of the sample

Figure 5: (Left) Ground surfaces of the cut, (Center and right) Initial crack

3.2 Experiment Preparation

3.2.1 Determination of the Frictional Coefficient

The frictional coefficient of the material after grinding was determined by placing two blocks ground in the same way together and then tilting them until the top block slides. The geometry of the samples are 70.0mm, 14.0mm, 20.0mm and 120.0mm, 200.0mm, 5.0mm. The angle when the upper sample slips is θ, then the frictional coefficient f is $f = tan\theta$. Based on the measurement data, the average angle θ is 30.15degrees, the frictional coefficient was therefore determined as *tan* (30.15) = 0.58.

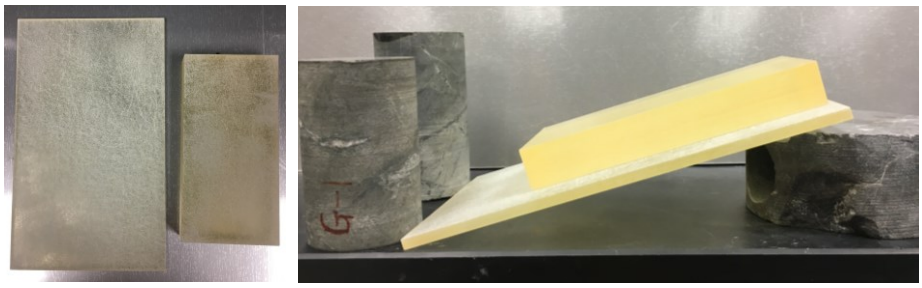

Figure 6: Samples used to measure the frictional coefficient

3.2.2 Determination of the Stress Intensity Factor of the Initial Crack

The first experiment was done to find the parameters to make an initial fracture propagate by water pressure. In this experiment, sample size and initial crack size were different from later experiments. The sample size is 50.0mm diameter by 100.0mm height as shown in

Figure **7**. An initial crack is printed on the bottom. The geometry of the initial crack is a half ellipsoid whose principal semiaxes are 20.0mm, 20.0mm, and 0.5mm.

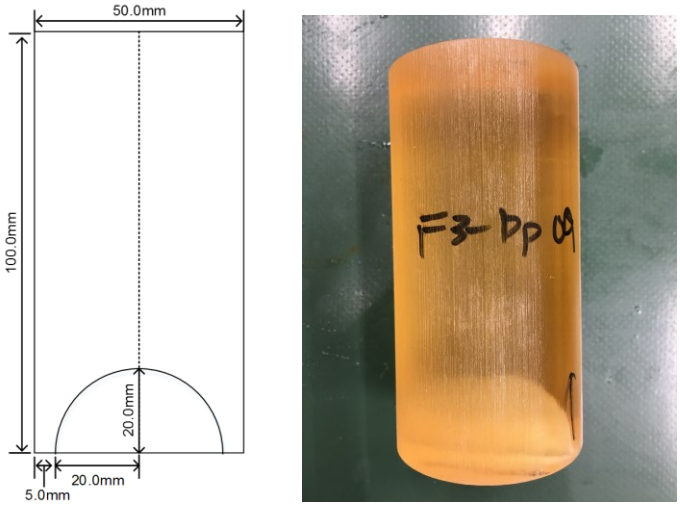

Figure 7: (Left) A sketch of the sample, (Right) The sample used in this experiment

The stress intensity factor of this ellipsoid was estimated. Murakami and Nemat-Nasser (1983) suggested that the critical stress intensity factor for a two-dimensional crack is proportional to the biquadratic root of its area. The equation derived empirically by them is:

$$K_{I\,max} = 0.629\sigma'_n\sqrt{\pi\sqrt{area}} \tag{17}$$

where σ'_n is the effective normal stress and area is the area of the crack.

The stress intensity factor of semielliptical cracks can be calculated (Anderson, 2005):

$$K_{I\,max} = \lambda_s\sigma'_n\sqrt{\frac{\pi a}{Q}}f(\phi) \tag{18}$$

$$Q = 1 + 1.464(\frac{a}{c})^{1.65} \tag{19}$$

$$\lambda_s = (1.13 - 0.09\frac{a}{c})(1 + 0.1(1 - \sin\phi)^2) \tag{20}$$

where a is the principal semiaxis perpendicular to the straight line of the semiellipse, c is the principal semiaxis parallel to the straight line of the semiellipse, and ϕ is the angle from the center point. However, these equations are only valid for a semiellipse where $a \leq c$.

Water was injected into the initial crack and the pressure was increased until it reached 25MPa. When the effective normal stress σ'_n was 22MPa, acoustic emission was detected and water injection was stopped immediately. A hydraulic fracture propagated for 50 – 66 mm at this water pressure as shown in Figure 8.

When a = c = 20.0 [mm] and σ'_n = 22 [MPa], K_I= 3.88 [$MPa\sqrt{m}$] based on Murakami and Nemat-Nasser (1983), or K_I= 3.28 [$MPa\sqrt{m}$] based on Anderson (2005). Based on these results, the critical stress intensity factor of the material is estimated to be around 3.3 – 3.9 $MPa\sqrt{m}$. The critical stress intensity factors of polymers generally range from 0.3 – 4.0 $MPa\sqrt{m}$. The estimated value is within this general range.

Table 3: Stress property during the experiment

Property	Value	Unit
Axial Stress	30	MPa
Confining Stress	3	MPa
Fluid Pressure	3-25	MPa

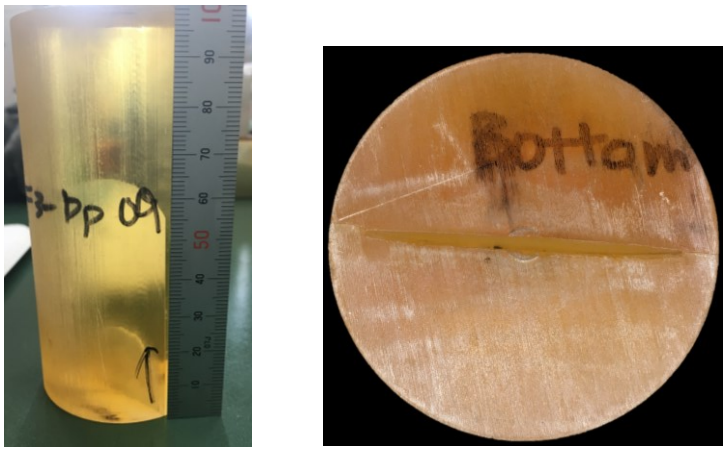

Figure 8: The sample after hydraulic fracturing

3.3 Numerical Results

The same parameters for this lab experiment were entered into the numerical model described in the previous section. For a precut intersecting orthogonally to a hydraulic fracture, a hydraulic fracture is expected to terminate at $\sigma_H = 20MPa$ and it is expected to cross at $\sigma_H = 60MPa$. When $\sigma_H = 40MPa$, the condition is categorized as pattern 3, which means half of the time, a hydraulic fracture would cross the precut.

Table 4: Parameters used in the numerical experiment

Parameters		Value	Unit
Maximum Horizontal Stress	σ_H	3 - 60	MPa
Least Horizontal Stress	σ_h	3	MPa
Fracture Intersecting Angle	θ	15 - 90	degrees
Mode-I Critical Stress Intensity Factor	K_I	3.5	$MPa \cdot \sqrt{m}$
Frictional Coefficient	f	0.58	-
Cohesion	S_0	0	MPa
Tensile Strength	T_0	50	MPa

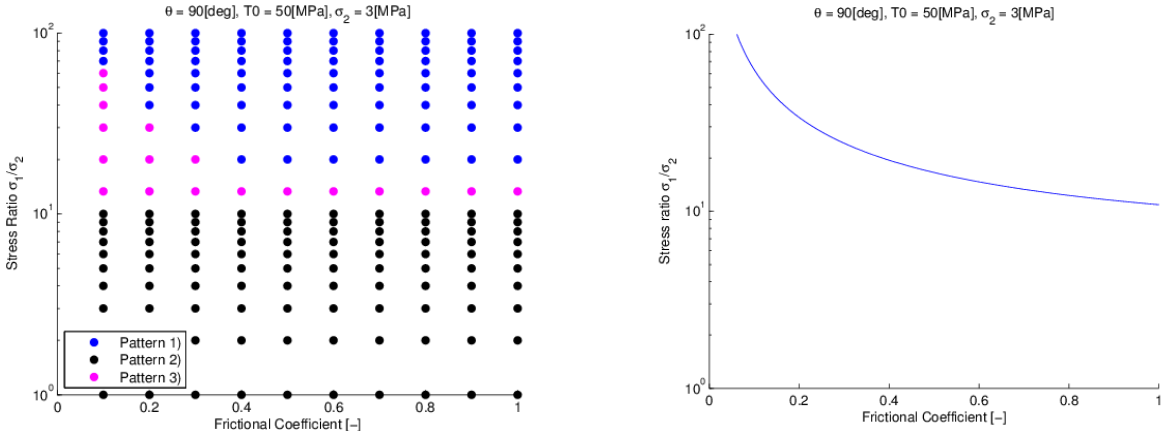

Figure 9: (Left) Numerical results with parameters in Table 4 and the varied stress ratio and the fracture angle. A hydraulic fracture is expected to cross in the area with blue dots, it is expected to terminate in the area with black dots, and pink dots show the area categorized in pattern3, where a propagating fracture is expected to cross half of the cases. (Right) Analytical results of Renshaw and Pollard (1995) with parameters in Table 4. A propagating fracture is expected to cross in the area above the line.

3.4 Experimental Results

During the experiments, we applied the axial stress and the confining pressure simultaneously until they reached the set values, then pure water was injected into the initial hydraulic fracture printed at the bottom of the sample. The water pressure was increased from 0MPa to 25MPa, and water injection was stopped immediately after we observed acoustic emission exceeding a certain threshold of amplitude where we assumed hydraulic fracturing occurred. In this work, we fixed the confining pressure, the frictional coefficient of the preexisting fracture, and the geometry of the initial hydraulic fracture. We changed axial stress in each experiment and observed whether a propagating fracture crosses or stops at the preexisting fracture. The results are discussed in the following sections in detail. The summary of the results is shown in Table 5.

Table 5: The summary of the experiment results

Test Case	σ_H [MPa]	σ_h [MPa]	Result	Numerical result
1	20	3	Stops	Pattern 2 (Stops)
2	40	3	Crosses	Pattern 3 (Sometimes crosses)
3	40	3	Stops	Pattern 3 (Sometimes crosses)

3.3.1 Test Case 1

The result of the cross/follow determination method shown in this paper for this test case suggests that a hydraulic fracture would follow a preexisting cut. In addition, the analytical criterion derived by Renshaw and Pollard (1995) shows the crossing/terminating threshold for the fracture intersecting the fracture with $\theta = \frac{\pi}{2}$ is:

$$\frac{-\sigma_{xx}^{r}}{T_0-\sigma_{yy}^{r}} > \frac{0.35+\frac{0.35}{\mu}}{1.06} \tag{21}$$

Here, σ_{xx}^{r} corresponds to the axial stress and σ_{yy}^{r} corresponds to the confining pressure in this setting. The frictional coefficient μ is 0.58 and tensile strength is 40-55MPa. The right hand side of the equation is 0.8995 ≈ 0.9. The left hand side of the equation is:

$$\frac{-\sigma_{xx}^{r}}{T_0-\sigma_{yy}^{r}} = \frac{20}{(40\ to\ 55)+3} = 0.345\ to\ 0.465 \tag{22}$$

The propagating fracture is therefore expected to stop at a preexisting fracture under these stress conditions, both by the analytical and numerical prediction.

The measurement data during the test are shown in Figure 10. The axial stress and the confining pressure were applied simultaneously until they reached the set values. Then water was injected at a constant rate of 5ml/min until we observed acoustic emission exceeding a certain threshold of amplitude where we assumed hydraulic fracturing occurred. The acoustic emission was detected at 654.32 second, when the axial stress was 20.07 MPa, the confining pressure was 3.00 MPa, and the water pressure was 18.42 MPa. After hydraulic fracturing occurred, the water pressure and the confining pressure became close in value, which means that the water and the oil used to apply the confining pressure were connected mechanically inside the triaxial machine.

Figure 11 shows the sample after the experiment. A hydraulic fracture propagated to the preexisting fracture, however, it stopped propagating at the interface and did not cross. This result is consistent with the analytical and numerical predictions.

Table 6: Stress properties during the experiment

Property	Value	Unit
Axial Stress	20	MPa
Confining Pressure	3	MPa
Fluid Pressure	3-25	MPa
Fracture Intersecting Angle	90	degrees

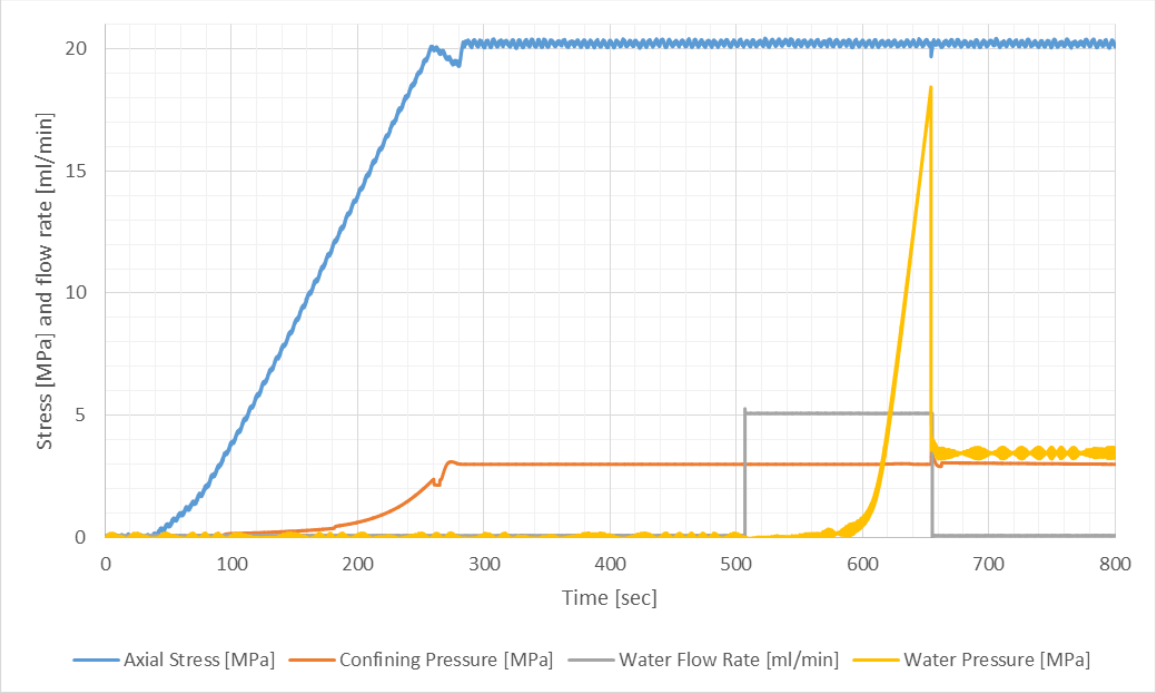

Figure 10: Pressure profiles and water flow rate during the experiment

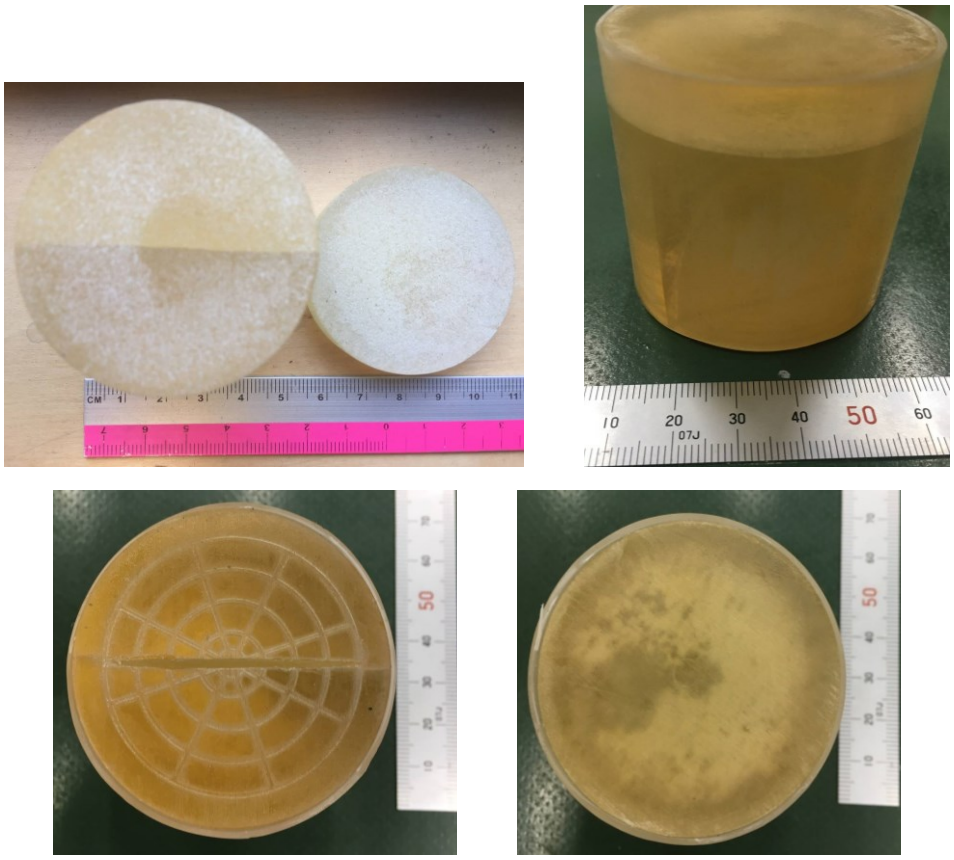

Figure 11: The sample after experiment

3.3.2 Test Case 2

The result of the cross/follow determination method shown here for this test case suggests that a hydraulic fracture would cross a preexisting cut when T_0 = 55MPa. Using the analytical criterion derived by Renshaw and Pollard (1995) , the crossing criterion is:

$$\frac{-\sigma_{xx}^r}{T_0 - \sigma_{yy}^r} > \frac{0.35 + \frac{0.35}{\mu}}{1.06} \tag{23}$$

The right hand side of the equation is 0.90. The left hand side of the equation is:

$$\frac{-\sigma_{xx}^r}{T_0 - \sigma_{yy}^r} = \frac{40}{(40\ to\ 55)+3} = 0.690\ to\ 0.930 \tag{24}$$

Consequently, the propagating fracture is expected to cross a preexisting fracture when T_0 > 43MPa and it is expected to follow in the case when T_0 < 43MPa under these stress properties. The numerical result shows that this condition is categorized as pattern 3, which means half of the time, a hydraulic fracture would cross the precut.

The measurement data obtained during the test are shown in Figure 13. The axial stress and the confining pressure were applied simultaneously until they reached the set values. Then water was injected at a constant rate of 5ml/min until we detected acoustic emission exceeding a certain threshold of amplitude where we assumed hydraulic fracturing occurred. The acoustic emission was observed at 1334.7 second, when the axial stress was 40.08 MPa, the confining pressure was 3.00 MPa, and the water pressure was 25.07 MPa. Figure 12 shows the sample after the experiment. A hydraulic fracture propagated to the preexisting fracture, and it crossed the interface and continued propagating.

Our original plan was to increase the axial stress to 60 MPa, where a propagating fracture is expected to cross based on numerical and analytical solutions. However, when we increased the axial stress near to 60MPa around 400 to 600sec (Figure 13), we observed that the vertical deformation increased significantly. We decreased the axial stress down to 30MPa then increased it and kept at 40MPa, where the vertical deformation was within a reasonable amount.

Table 7: Stress property during the experiment

Property	Value	Unit
Axial Stress	40	MPa
Confining Stress	3	MPa
Fluid Pressure	3-25	MPa
Fracture Intersecting Angle	90	degrees

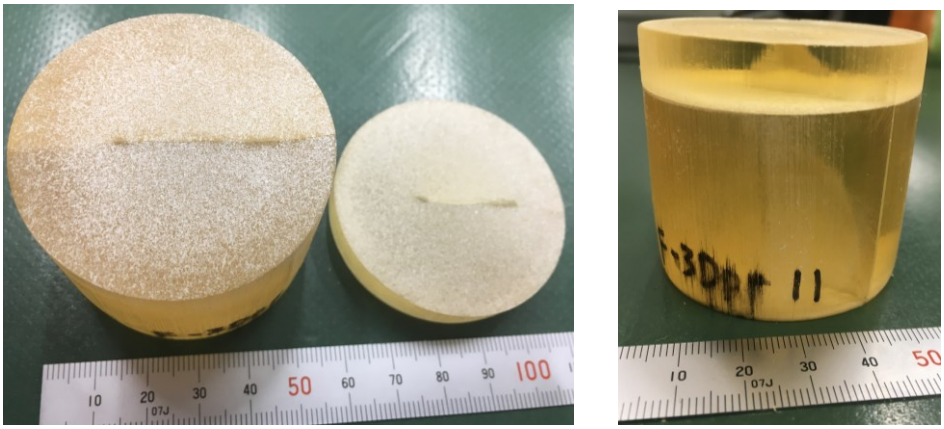

Figure 12: The sample after the experiment

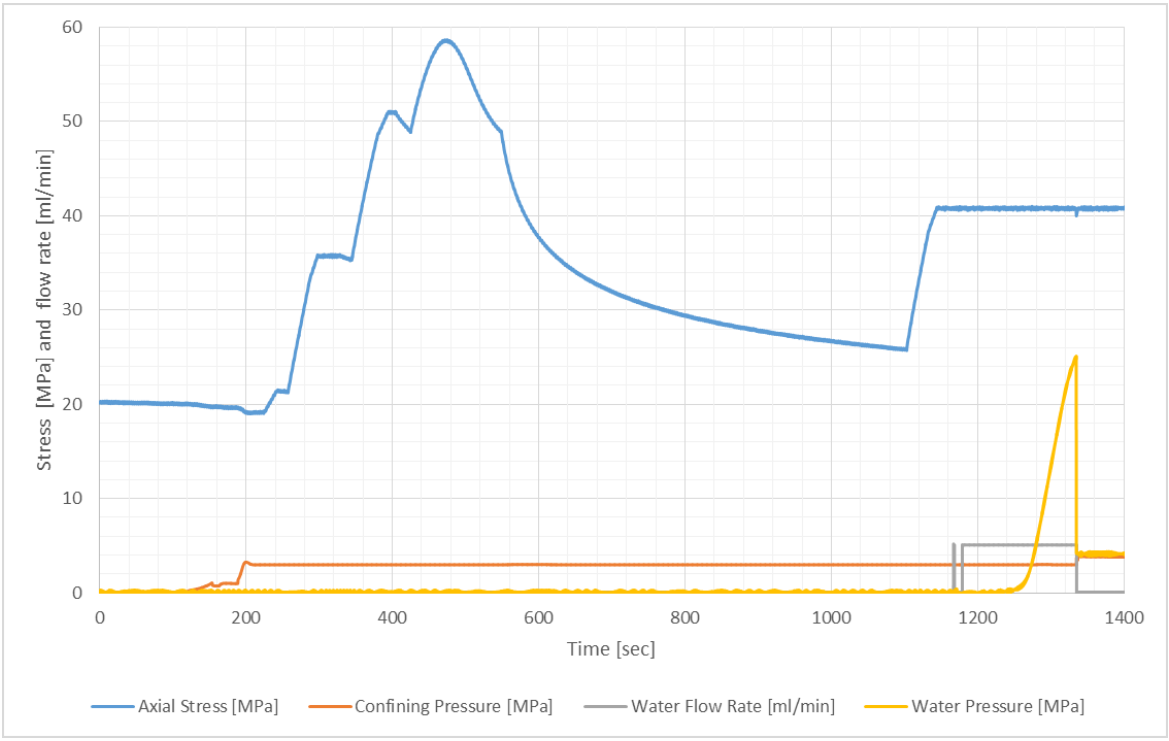

Figure 13: Pressure profiles and water flow rate during the experiment

3.3.2 Test Case 3

During test case 2, we observed that the sample started yielding when axial stress was around 55MPa. To avoid plastic strain, we increased the axial stress from 0MPa to 40MPa directly this time and tested it with the same settings again.

Table 8: Stress property during the experiment

Property	Value	Unit
Axial Stress	40	MPa
Confining Stress	3	MPa
Fluid Pressure	3-25	MPa
Fracture Intersecting Angle	90	degrees

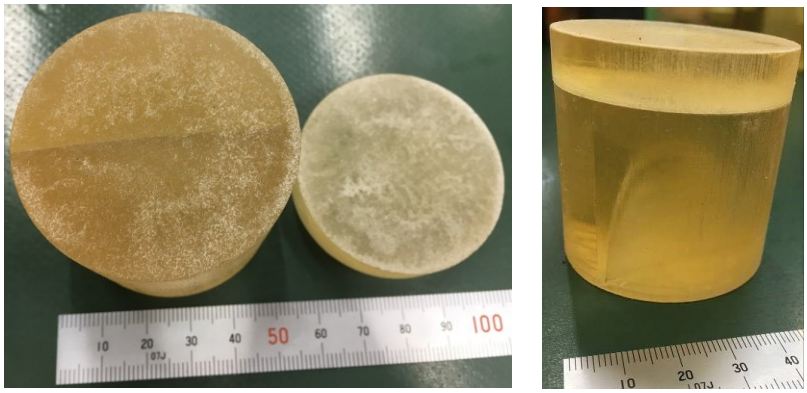

Figure 14: The sample after experiment

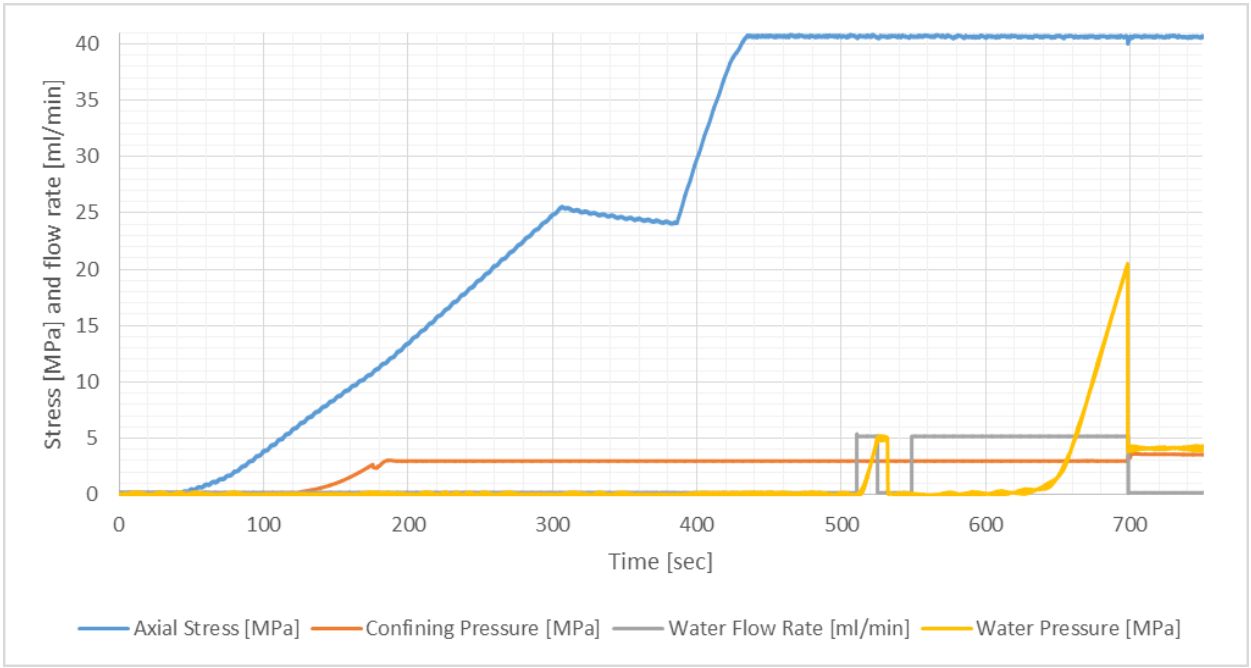

Figure 15: Pressure profiles and water flow rate during the experiment

The measurement data during the test are shown in Figure 15. The acoustic emission was observed at 698.32 second, when the axial stress was 40.62 MPa, the confining pressure was 3.00 MPa, and water pressure was 20.5 MPa.

Figure 14 shows the sample after the experiment. A hydraulic fracture propagated to the preexisting fracture, and it did not cross the interface and stopped propagating. This result is consistent with the analytical and numerical results, assuming that the tensile strength was larger than 43MPa.

3.5 Discussion

The results of the hydraulic fracturing experiment using 3D-printed samples show good agreement with the numerical results and the analytical criterion of Renshaw and Pollard (1995). The reason why the results of the test case 2 and 3 were different could be because the sample in test case 2 was applied a higher axial stress. The sample expanded horizontally and contracted vertically after the experiment. We suppose that the sample started yielding when the axial stress was near to 60MPa and it led to this remaining plastic deformation. The remaining deformation would cause residual stress in the sample, which could affect the result.

Our results also demonstrate the possibilities of using 3D-printed core samples for fracturing experiments. There are several specific advantages of using 3D-printed samples. The transparent material enables us to observe how a fracture spreads in the core without breaking it open to see. The highly homogeneous material without any flaws is ideal for a fracturing experiment. The geometries of the initial crack and the precut can be designed precisely, making it potentially useful for more complex fracturing experiments. However, the low compressive strength and the yield strength limited the axial stress that could be applied to the sample, which made it difficult to create the conditions where a propagating fracture would cross a precut. It would be possible to extend this experiment using cement which has much higher compressive strength and yield strength and lower tensile strength. Higher compressive strength would enable the application of higher axial stress, and a wider range of stress state could then be applied to a sample. This would enable test of precuts with arbitrary angles. Lower tensile strength enables a sample to be hydraulically fractured with lower fluid pressure, which gives room to apply higher confining pressure. Our next step is to continue the experiment with cement or other suitable material to investigate a propagating fracture intersecting another fracture at arbitrary angle.

4. CONCLUSION

In this study, as an approach to model hydraulic stimulation in an EGS reservoir, a numerical model to determine whether a propagating fracture crosses or follows a preexisting natural fracture was developed and verified by comparing to experimental data in previous studies. In addition, laboratory scale experiments were conducted to verify the numerical model and also explore the possibility of using 3D-printed core samples for hydraulic fracturing experiments.

To investigate fracture network creation, physics-based approaches including fluid flow and geomechanics that can simulate fracture propagation and stimulation at a field scale will be necessary. The numerical model introduced in this study will be the first step toward understanding a fracture network creation and will be combined in future work with other geomechanical models to tackle this problem.

ACKNOWLEDGEMENTS

This research was supported by the Ito Foundation for International Education Exchange, by Ms. Margot Leidig through the grant of the Calvin Enderlin Earth Sciences Fellowship, and by the industrial affiliates at the Stanford Center for Induced and Triggered Seismicity. This research was also supported by METI, Japan through International Research Program for Innovative Energy Technology.

REFERENCES

Anderson, T. L. : *Fracture Mechanics.* Boca Raton: CRC Press, (2005), https://doi.org/10.1201/9781420058215.

Blanton, T. L.: An Experimental Study of Interaction Between Hydraulically Induced and Pre-Existing Fractures. *Society of Petroleum Engineers,* (1982), doi:10.2118/10847-MS

Chen, Z., Yang, Z., & Wang, M.: Hydro-mechanical coupled mechanisms of hydraulic fracture propagation in rocks with cemented natural fractures. *Journal of Petroleum Science and Engineering*, *163* (January), 421–434. (2018). http://doi.org/10.1016/j.petrol.2017.12.092

Gu, H., & Weng, X. : Criterion for Fractures Crossing Frictional Interfaces at Non-orthogonal Angles. *American Rock Mechanics Association*, (2010),

Gu, H., Weng, X., Lund, J., Mack, M., Ganguly, U., & Suarez-Rivera, R. : Hydraulic Fracture Crossing Natural Fracture at Non-orthogonal Angles, A Criterion, Its Validation and Applications, *Society of Petroleum Engineers*, (2011), doi:10.2118/139984-PA

Helgeson, D. E., & Aydin, A. : Characteristics of joint propagation across layer interfaces in sedimentary rocks. *Journal of Structural Geology*, *13*(8), 897–911, (1991)

McClure, M. W. : Stimulation Mechanism and the Direction of Propagation of Microseismicity. *PROCEEDINGS, Thirty-Ninth Workshop on Geothermal Reservoir Engineering Stanford University,* (2014).

McClure, M. W., & Horne, R. N. : An investigation of stimulation mechanisms in Enhanced Geothermal Systems. *International Journal of Rock Mechanics and Mining Sciences*, *72*, 242–260, (2014), http://doi.org/10.1016/j.ijrmms.2014.07.011

Murakami, Y., & Nemat-Nasser, S.: Growth and stability of interacting surface flaws of arbitrary shape. *Engineering Fracture Mechanics*, *17*(3), 193–210. (1983), http://doi.org/10.1016/0013-7944(83)90027-9

Norbeck, J. H.: Hydromechanical and frictional faulting behavior of fuluidinjuctioninduced earthquake. *Stanford PhD Dissertation*,

(2016).

Norbeck, J. H., Mcclure, M. W., & Horne, R. N. : Revisiting Stimulation Mechanism at Fenton Hill and an Investigation of the Influence of Fault Heterogeneity on the Gutenberg-Richter b-value for Rate-and-State Earthquake Simulations. *PROCEEDINGS Geothermal Reservoir Engineering Stanford University*, (2016).

Olson, J. E.: Multi-fracture propagation modeling: Applications to hydraulic fracturing in shales and tight gas sands. *The 42nd US Rock Mechanics Symposium*. (2008).

Pollard, D. D., & Fletcher, R. C.: *Fundamentals of structural geology*. Cambridge University Press, (2005). doi: 10.2277/0521839270

Renshaw, C. E., & Pollard, D. D.: An Experimentally Verified Criterion for Propagation Across Unbounded Frictional Interfaces in Brittle, Linear Elastic Materials. *J. Rock Mech. Min. Sci. & Geomech. Abstr*, *32*(3), 237–249, (1995).

Segall, P.: *Earthquake and volcano deformation*. Princeton University Press, (2010).

Warpinski, N. R., & Teufel, L. W.: Influence of Geologic Discontinuities on Hydraulic Fracture Propagation, *Society of Petroleum Engineers,* (1987), doi:10.2118/13224-PA

Weng, X., Kresse, O., Cohen, C., Wu, R., & Gu, H.: Modeling of Hydraulic-Fracture-Network Propagation in a Naturally Fractured Formation, *Society of Petroleum Engineers,* (2011), doi:10.2118/140253-PA

Wu, H., & Pollard, D. D.: Propagation of a set of opening-mode fractures in layered brittle materials under uniaxial strain cycling. *Journal of Geophysical Research: Solid Earth*, *97*(B3), 3381–3396. (1992), http://doi.org/10.1029/91JB02857

Zhou, J., Chen, M., Jin, Y., & Zhang, G.-Q.: Analysis of fracture propagation behavior and fracture geometry using a tri-axial fracturing system in naturally fractured reservoirs. *International Journal of Rock Mechanics & Mining Sciences*, *45*, 1143–1152. (2008)., http://doi.org/10.1016/j.ijrmms.2008.01.001

Zoback, M. D.: *Reservoir geomechanics*. Cambridge University Press. (2007).